DOI 10.1515/hsz-2012-0252 — Biol. Chem. 2012; 393(12): 1405–1416

Stefanie R. Mullins[a], Mansoureh Sameni, Galia Blum[b], Matthew Bogyo, Bonnie F. Sloane and Kamiar Moin*

Three-dimensional cultures modeling premalignant progression of human breast epithelial cells: role of cysteine cathepsins

Abstract: The expression of the cysteine protease cathepsin B is increased in early stages of human breast cancer. To assess the potential role of cathepsin B in premalignant progression of breast epithelial cells, we employed a 3D reconstituted basement membrane overlay culture model of MCF10A human breast epithelial cells and isogenic variants that replicate the *in vivo* phenotypes of hyperplasia (MCF10AneoT) and atypical hyperplasia (MCF10AT1). MCF10A cells developed into polarized acinar structures with central lumens. In contrast, MCF10AneoT and MCF10AT1 cells form larger structures in which the lumens are filled with cells. CA074Me, a cell-permeable inhibitor selective for the cysteine cathepsins B and L, reduced proliferation and increased apoptosis of MCF10A, MCF10AneoT and MCF10AT1 cells in 3D culture. We detected active cysteine cathepsins in the isogenic MCF10 variants in 3D culture with GB111, a cell-permeable activity-based probe, and established differential inhibition of cathepsin B in our 3D cultures. We conclude that cathepsin B promotes proliferation and premalignant progression of breast epithelial cells. These findings are consistent with studies by others showing that deletion of cathepsin B in the transgenic MMTV-PyMT mice, a murine model that is predisposed to development of mammary cancer, reduces malignant progression.

Keywords: activity-based probes; breast cancer; cysteine cathepsins; premalignant progression; protease inhibitors.

[a]Present Address: MedImmune, Cambridge, UK
[b]Present Address: School of Pharmacy, Institute for Drug Research, Hebrew University of Jerusalem, Jerusalem, Israel
***Corresponding author: Kamiar Moin,** Barbara Ann Karmanos Cancer Institute, Wayne State University School of Medicine, Detroit, MI 48201, USA; and Department of Pharmacology, Wayne State University School of Medicine, Detroit, MI 48201, USA, e-mail: kmoin@wayne.edu
Stefanie R. Mullins: Barbara Ann Karmanos Cancer Institute, Wayne State University School of Medicine, Detroit, MI 48201, USA
Mansoureh Sameni: Department of Pharmacology, Wayne State University School of Medicine, Detroit, MI 48201, USA
Galia Blum: Departments of Microbiology & Immunology and Pathology, Stanford University School of Medicine, Stanford, CA 94305, USA
Matthew Bogyo: Departments of Microbiology & Immunology and Pathology, Stanford University School of Medicine, Stanford, CA 94305, USA
Bonnie F. Sloane: Barbara Ann Karmanos Cancer Institute, Wayne State University School of Medicine, Detroit, MI 48201, USA; and Department of Pharmacology, Wayne State University School of Medicine, Detroit, MI 48201, USA

Introduction

Cysteine cathepsins are papain-like cysteine proteases that function in protein turnover and degradation within endosomal-lysosomal vesicles (for reviews see Mohamed and Sloane, 2006; Reiser et al., 2010; Turk et al., 2012). Studies in knockout mice have identified both unique and redundant physiological functions for these cysteine cathepsins. For example, cathepsin B-deficient mice appear normal, yet are resistant to pathological stresses such as pancreatitis and liver injury (Halangk et al., 2000; Guicciardi et al., 2001). In cathepsin L-deficient mice there is hyperproliferation of keratinocytes, resulting in disregulation of their hair cycle because of altered trafficking of EGF and the EGF receptor, as well as progressive dilated cardiomyopathy (Reinheckel et al., 2005). When cathepsin B- and L-deficient mice are crossed, they develop severe brain and neural abnormalities that result in death shortly after birth (Felbor et al., 2002).

Cysteine cathepsins have been implicated in diseases such as atherosclerosis, osteoarthritis and osteoporosis. Cathepsin K inhibitors are in clinical trials for the treatment of osteoporosis, osteoarthritis and bone metastasis, caused by the high levels of expression of cathepsin K in osteoclasts and the role of this enzyme in bone resorption (Felbor et al., 2002; Abbenante and Fairlie, 2005). Inhibitors of cathepsin S have been tested for the treatment of psoriasis and osteoarthritis (Yasuda et al., 2005). In addition, cysteine cathepsins are being studied as potential diagnostic targets.

Cathepsin L and S appear to be promising biomarkers for atherosclerosis because of their increased expression in the serum of patients with atherosclerotic stenosis (Liu et al., 2006a, b; Lutgens et al., 2007; Reiser et al., 2010). Cathepsin B is being targeted for diagnostic imaging in atherosclerosis and cancer (Chen et al., 2002; Alencar et al., 2007). In a xenograft model of colon cancer, a cathepsin B-activated smart near-infrared probe accumulating in the tumor, detected 30-fold greater enzyme activity than in control animals (Alencar et al., 2007), suggesting the potential promise of diagnostic imaging of cathepsin B.

Seven cysteine cathepsins have been linked to breast cancer progression: cathepsins B, L, H, K, S, V and X (for review see Watson and Kreuzaler, 2009). Microarray analyses identified cathepsin B as a gene which is highly expressed in ductal breast carcinoma as compared with lobular breast carcinoma (Wulfkuhle et al., 2002; Korkola et al., 2003). Proteomic analyses of matched normal and ductal carcinoma *in situ* breast tissue revealed an increase in the expression of cathepsin B protein in premalignant ductal carcinoma *in situ* lesions (Zajc et al., 2002). Comparison of the MCF-10F breast epithelial cell line to the same cell line transformed with the c-Ha-ras oncogene and then treated with DMBA (7,12-dimethylbenz[a]anthracene) demonstrated that both cathepsin B and cathepsin L protein levels increase in parallel with an increase in invasiveness (Premzl et al., 2001). Indeed a role for cysteine cathepsins in breast cancer invasion was postulated because of the ability of these enzymes to degrade extracellular matrix (Obermajer et al., 2008) and was shown for cathepsin B in the invasion of MCF10A variants by using small molecule inhibitors selective for cathepsin B (Bervar et al., 2003).

Animal studies have indicated that cysteine cathepsins may be involved at an earlier stage in tumor progression than invasion. For example, in a transgenic mouse model for pancreatic islet carcinogenesis – RIP1-Tag2 – a role for cysteine cathepsins in proliferation, tumor growth and vascularity, as well as invasion, was demonstrated (Joyce et al., 2004; Gocheva et al., 2006; Vasiljeva et al., 2006; Wang et al., 2006). In the MMTV-PyMT transgenic mouse model of breast cancer, a deficiency in cathepsin B expression has been shown to decrease tumor onset and growth rate (Vasiljeva et al., 2006), whereas transgenic expression of cathepsin B has been shown to increase proliferation and promote progression (Sevenich et al., 2011).

Elegant studies by Bissell and colleagues have shown that 3D cultures of breast epithelial cells can be used to analyze morphogenesis and functional differentiation (Lo et al., 2012) and 3D cultures of breast cancer cells are predictive of clinical outcome (Martin et al., 2008). We and our colleagues (Li et al., 2010) have shown that 3D cultures of breast cells can be used to analyze kinase pathways and resistance to cytotoxic therapy. In the present study, we analyzed the morphogenesis of a series of isogenic cell lines that represent stages prior to and early in premalignant progression: the non-tumorigenic MCF10A, c-H-ras transformed MCF10AneoT (Basolo et al., 1991; Miller et al., 1993) and non-invasive MCF10AT1 (Miller et al., 1993) and the role of cysteine cathepsins in the morphogenesis of these lines. We grew the MCF10A variants in 3D reconstituted basement membrane (rBM) overlay cultures, using methods optimized by Brugge and colleagues (Debnath et al., 2003, 2005) for analysis of the morphogenesis of MCF10A cells, and found that a selective inhibitor that targets intracellular cathepsin B reduced proliferation and increased apoptosis.

Results

Three-dimensional rBM overlay cultures model premalignant progression of breast epithelium

We extended the 3D rBM overlay culture system developed by Brugge and colleagues for MCF10A cells (Debnath et al., 2003) to include premalignant isogenic 10A variants, i.e., MCF10AneoT and MCF10AT1. As a baseline, we first established the levels of expression and localization of cathepsin B in the MCF10 variants at various time points (Supplementary Figure 1). We also confirmed that, in our hands, the MCF10A cells develop into polarized acini (Figure 1A–C) in which central lumens are surrounded by a single layer of epithelial cells (Figure 1A) and cells within the lumen undergo apoptosis (Figure 1B). We have shown previously that MCF10A cells form polarized structures by staining for β1 integrin (Sameni et al., 2012 in press). Here, we confirm formation of polarized acini by staining for the basal marker α6 integrin (Figure 1B) (Nedvetskey et al., 2012). The MCF10AneoT and MCF10AT1 cells, in contrast to the MCF10A cells, grow into larger structures that lack a central hollow lumen (Figure 1D–E, respectively). MCF10AT1 cells can also form multi-acinar structures that do not have central lumens (Li et al., 2008) (Figure 1F–G). This is consistent with the behavior of these cells *in vivo* as subcutaneous xenografts where MCF10AneoT and MCF10AT1 cells form simple ducts that progress to benign hyperplastic and atypical hyperplastic lesions, respectively (Dawson et al., 1996). Thus, we have in hand an *in vitro* model system that recapitulates the premalignant progression of breast epithelium.

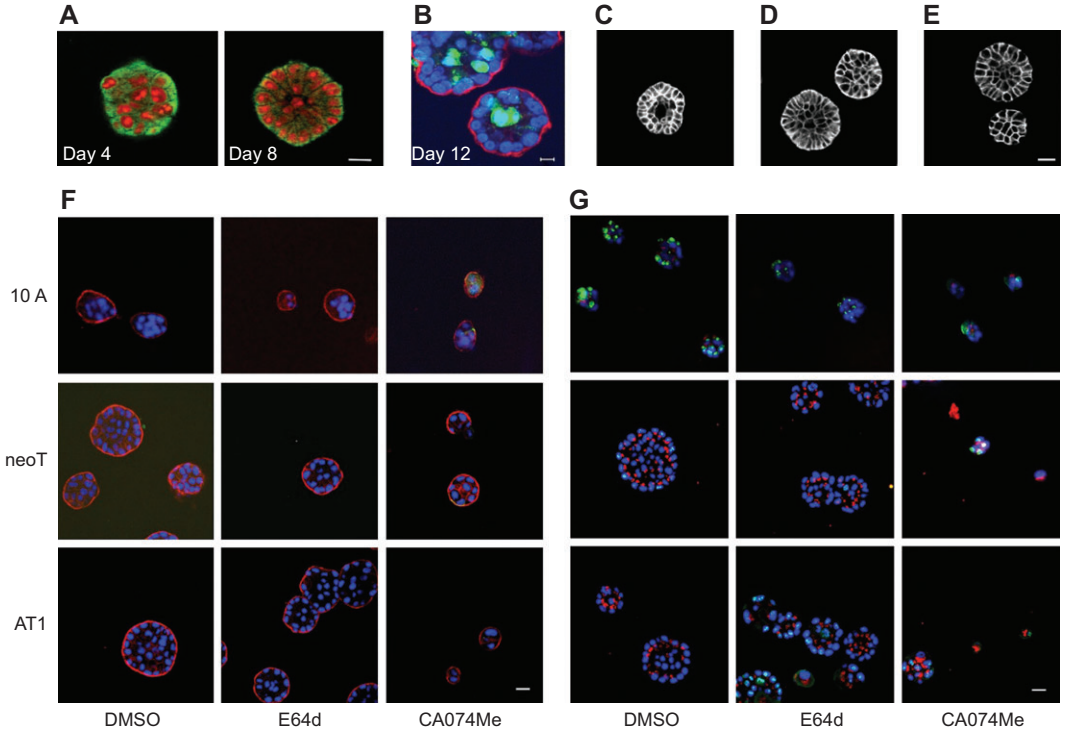

Figure 1 In 3D rBM overlay culture, MCF10A cells form polarized acini with hollow central lumens (A–C), whereas MCF10AneoT (D) and MCF10AT1 (E) cells do not.
Structures in (A) were stained for smooth muscle actin (phalloidin, green) and nuclei (propidium iodide, red). Bars, 20 μm. In 12-day cultures (B), apoptosis of cells in the central lumen, as shown by staining for cleaved caspase 3 (green), was observed. Nuclei (DAPI, blue) were located adjacent to the basal membrane, which is stained here for α6 integrin (red). Bar, 10 μm. (C–E) depict optical sections, taken at the equatorial plane of representative structures at 8 days of culture, of the actin cytoskeleton (phalloidin) of MCF10A, MCF10AneoT and MCF10AT1 structures, respectively. Bar, 20 μm. Panels (F) and (G) show that protease inhibitors did not affect the development of MCF10A isogenic variants in 3D rBM overlay culture. Immunofluorescence staining was performed on day 4 structures using antibodies against (F) α6 integrin (red) and cleaved caspase 3 (green) or (G) GM130 (red) and Ki67 (green). Nuclei were stained with DAPI (blue). Cells were grown in the presence of 0.1% DMSO, 5 μM E64d or 5 μM CA074Me. Images represent a single confocal section at the equatorial plane of the structures. Bar, 20 μm.

Effect of cysteine protease inhibitors on MCF10A variants in 3D rBM overlay culture

Proteases of multiple classes including cysteine cathepsins have been implicated in the normal physiology and pathogenesis of the mammary gland (Khokha and Werb, 2011; Sloane, 2012). When cathepsin B-deficient mice are crossed with MMTV-PyMT mice that are predisposed to development of mammary carcinomas, the proliferation of primary tumors and lung metastases is reduced (Vasiljeva et al., 2008). In the skin, deficiencies in cathepsin L promote proliferation of keratinocytes (Reinheckel et al., 2005) and progression of squamous cell carcinoma (Dennemarker et al., 2010), suggesting that cathepsin L may play a protective or anti-tumor role. In a mouse model for pancreatic ductal adenocarcinoma, loss of cathepsin B leads to increases in the levels of active cathepsin L (Gopinathan et al., 2012). Thus, the interactions between these two cysteine cathepsins may regulate the proliferation of tumors.

We examined the effect of inhibiting cysteine cathepsin activity on the morphogenesis of MCF10 variants grown in 3D rBM overlay culture. The two inhibitors we used were: E-64d, a broad-spectrum cell-permeable inhibitor of cysteine proteases (McGowan et al. 1989; Wilcox and Mason 1992) and CA074Me, a selective cell-permeable inhibitor of cysteine cathepsins B and L (Montaser et al., 2002). At 4 days, we assessed the polarity by staining for the basal marker α6 integrin (Figure 1F) (Nedvetsky et al., 2012) and GM130, a marker for the apical orientation of the Golgi apparatus (Figure 1G); proliferation by staining for Ki67 (Figure 1G); and apoptosis by staining for cleaved caspase-3 (Figure 1F) (Debnath et al. 2003). Neither polarity nor apoptosis was affected by incubation with E64d or CA074Me. Similar results were obtained in cultures grown for 8, 12 and 16 days (data not shown). The presence of

Ki67 staining in cultures incubated with the protease inhibitors suggested that the cells remained able to proliferate. The size of structures formed by the MCF10 variants incubated with E64d was variable (Figure 1F and G). In contrast, the size of structures formed by the MCF10 variants incubated with CA074Me was much smaller than that of controls (Figure 1F and G).

To quantify the effect of the inhibitors on structure size, we measured the equatorial areas of ten structures after 8 days in culture (Figure 2). The broad-spectrum inhibitor, E64d, even at a 10-fold higher concentration than CA074Me, did not affect structure size. Conversely, structures grown in the presence of CA074Me were significantly smaller than control structures grown in the presence of the diluent. Cell-impermeable or non-methylated forms of E64d and CA074Me, i.e., E64 and CA074, did not affect proliferation of MCF10 variants in 3D rBM overlay culture (Table 1).

Because of the dramatically reduced size of structures in the presence of CA074Me, we also quantified the effect of inhibitor treatment on proliferation by measuring Ki67 expression (Figure 3). CA074Me significantly reduced the percentage of MCF10A and MCF10AT1 structures positive for Ki67 and showed a trend to reduction of the percentage of MCF10AneoT structures positive for Ki67 (Figure 3, left panel). These results are consistent with a decrease in cell proliferation being responsible for the smaller size of the structures. In contrast, E64d had no effect on the percentage of Ki67 positive structures (Figure 3, left panel). To determine whether the change in structure size might be related to increased apoptosis, we assessed the percentage of structures positive for cleaved caspase 3 for MCF10 variants grown in 3D rBM overlay culture in the presence and absence of cysteine protease inhibitors (Figure 3, right panel). The percentage of structures positive for cleaved caspase 3 was higher for all MCF10 variants, but only significantly elevated for the MCF10A and MCF10AT1 variants.

MTT [3-(4,5-dimethylthiazol-2-yl)-2,5 diphenyltetrazolium bromide] assays were performed to further analyze the effects of inhibitors on the proliferation of MCF10A, MCF10AneoT and MCF10AT1 cells. We first examined the effects in 2D monolayer cultures incubated with E64d or CA074Me at a series of concentrations. E64d did not affect proliferation (Supplementary Figure 2A). Only the highest concentration (10 μM) of CA074Me significantly inhibited the proliferation of MCF10A (Supplementary Figure 2B). Similar results were observed for MCF10AneoT and MCF10AT1 cells in 2D culture (data not shown). We adapted the MTT assays to the analysis of 3D rBM overlay cultures as described in Materials and methods. A 10 μM concentration of CA074Me reduced the proliferation of MCF10A, MCF10AneoT and MCF10AT1 cells in 3D rBM overlay culture (Figure 4). In contrast E64d at a concentration of 100 μM did not inhibit proliferation (Figure 4).

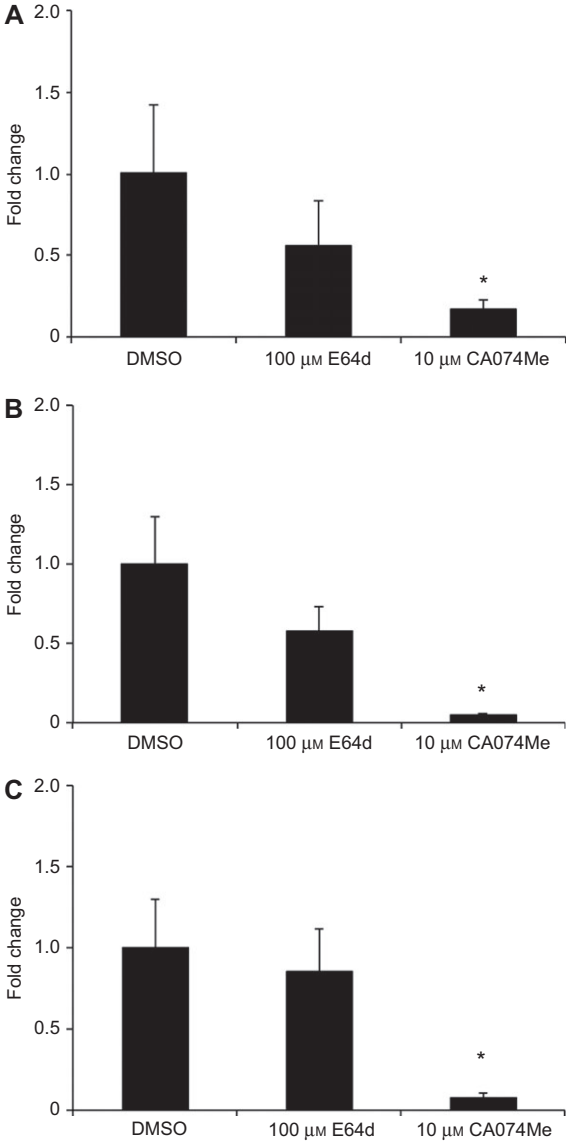

Figure 2 Sizes of structures formed by MCF10A (A), MCF10A neoT (B) or MCF10AT1 (C) cells are significantly reduced when grown for 8 days in the presence of CA074Me (10 μM).
The slight reduction in structure size in the presence of E64d (100 μM) was not significant. Equatorial areas of ten acini per treatment group were measured as described in Materials and methods. Data are expressed as fold change (mean±SD; *$p<0.001$) in the area of the structures treated with protease inhibitor as compared to the area of the structures treated with diluent 0.1% DMSO.

We also tested a variety of other protease inhibitors for their ability to affect cell proliferation using MTT assays (Table 1). Protease inhibitors shown to decrease cell proliferation were: PD150606, an inhibitor of calpains, a family of calcium-dependent cysteine proteases; GM6001,

Inhibitor	Target	Highest concentration tested	Inhibits proliferation
E64	Cysteine proteases	10 μM	–
E64d (intracellular)	Cysteine proteases	100 μM	–
CA074	CTSB	10 μM	–
CA074Me (intracellular)	CTSB, CTSL	50 μM	+
Cbz-Phe-Ser(OBzl)-CHN_2	CTSB, CTSL	20 μM	+
Cbz-Leu-Leu-Tyr-CHN_2	CTSB, CTSL, calpain	20 μM	+
Cbz-Phe-Phe(pNO_2)-CHN_2	CTSL	20 μM	–
Cbz-Phe-Tyr(OtBu)-CHN_2	CTSL	20 μM	–
PD 150606	Calpain	100 μM	+
GM6001	MMPs	100 μM	+
SB3CT	MMP-2 and -9, TACE	50 μM	+

Table 1 Effect of protease inhibitors on proliferation.

a broad-spectrum MMP inhibitor; SB3CT, an MMP inhibitor with selectivity toward MMP 2 and 9 (Kleifeld et al., 2001); and Cbz-Phe-Ser(OBzl)-CHN_2, a cysteine protease inhibitor with selectivity for cathepsins B and L (Seyfried et al., 2001). In contrast, two inhibitors of cathepsin L [Cbz-Phe-Phe(pNO_2)-CHN_2 and Cbz-Phe-Tyr(OtBu)-CHN_2] did not have any effect. These results implicate proteases in addition to cathepsin B in proliferation of the MCF10 variants. As the cell-impermeable cathepsin B inhibitor, CA074, and the cell-impermeable cysteine protease inhibitor, E64, did not have any effect, our results support intracellular rather than secreted cysteine cathepsins playing a role in proliferation of the MCF10 variants.

Effects of cysteine protease inhibitors on cell viability

We used calcein AM and ethidium homodimer-1 to differentiate live and dead cells, respectively, growing in 3D rBM overlay cultures of MCF10 variants (Supplementary Figure 3). Only a few dead cells could be observed in cultures incubated with inhibitors. As indicated above, the percentage of structures positive for cleaved caspase 3 was higher for all MCF10 variants, but only significantly elevated for the MCF10A and MCF10AT1 variants (Figure 3, right panel), confirming that the effect was not caused by an adverse effect of the inhibitor on the cells directly.

Defining targets of CA074Me and E64d in 3D rBM overlay cultures of MCF10 variants with activity-based probes

In the studies above, greater effects were observed in cultures incubated with CA074Me than with E64d. To determine whether our findings reflected differential effects of CA074Me and E64d on cathepsins B and L in the MCF10 variants grown in 3D rBM overlay culture, we used GB111, an activity-based probe (ABP) that covalently binds to the active site of cysteine cathepsins (Blum et al., 2005). The active cysteine cathepsins labeled by GB111 in the three MCF10 variants were of similar molecular size (Figure 5A). To identify the different molecular weight bands labeled by GB111 (Figure 5B, lane 3), we pretreated MCF10A 3D rBM overlay cultures with cysteine protease inhibitors and harvested cell lysates. We observed that 10 μM CA074Me reduced labeling of the 31 and 28 kDa bands (Figure 5B, lane 5), whereas 10 μM E64d reduced labeling of the 33 and 28 kDa bands (Figure 5B, lane 6). Even at a 10-fold higher concentration, pretreatment with E64d did not eliminate labeling of the 31 kDa band (Figure 5C). This band was presumed to represent the single chain active form of cathepsin B, which in tumors runs at ~31 kDa (Moin et al., 1992). Indeed, GB111 labeled a 31 kDa band in lanes containing the single chain active form of recombinant cathepsin B (Figure 5B, lane 1 and 5C, lane 7). We further verified that the 31 kDa band labeled by GB111 in the 3D cultures was cathepsin B by immunoprecipitation with a cathepsin B antibody (Figure 5D). In contrast to the observed differential efficacy in blocking binding of GB111 to 31 kDa single chain cathepsin B, CA074Me and E64d both blocked binding of GB111 to a 28 kDa band, which was verified to be cathepsin L by immunoprecipitation with a cathepsin L antibody (Figure 5E). GB111 labeling demonstrated that the targets of CA074Me and E64d in lysates of 3D rBM overlay cultures of MCF10neoT and MCF10AT1 cells were the same as in MCF10A cells (data not shown). Our results are consistent with E64d being less efficacious than CA074Me against cathepsin B (at least under the conditions studied here).

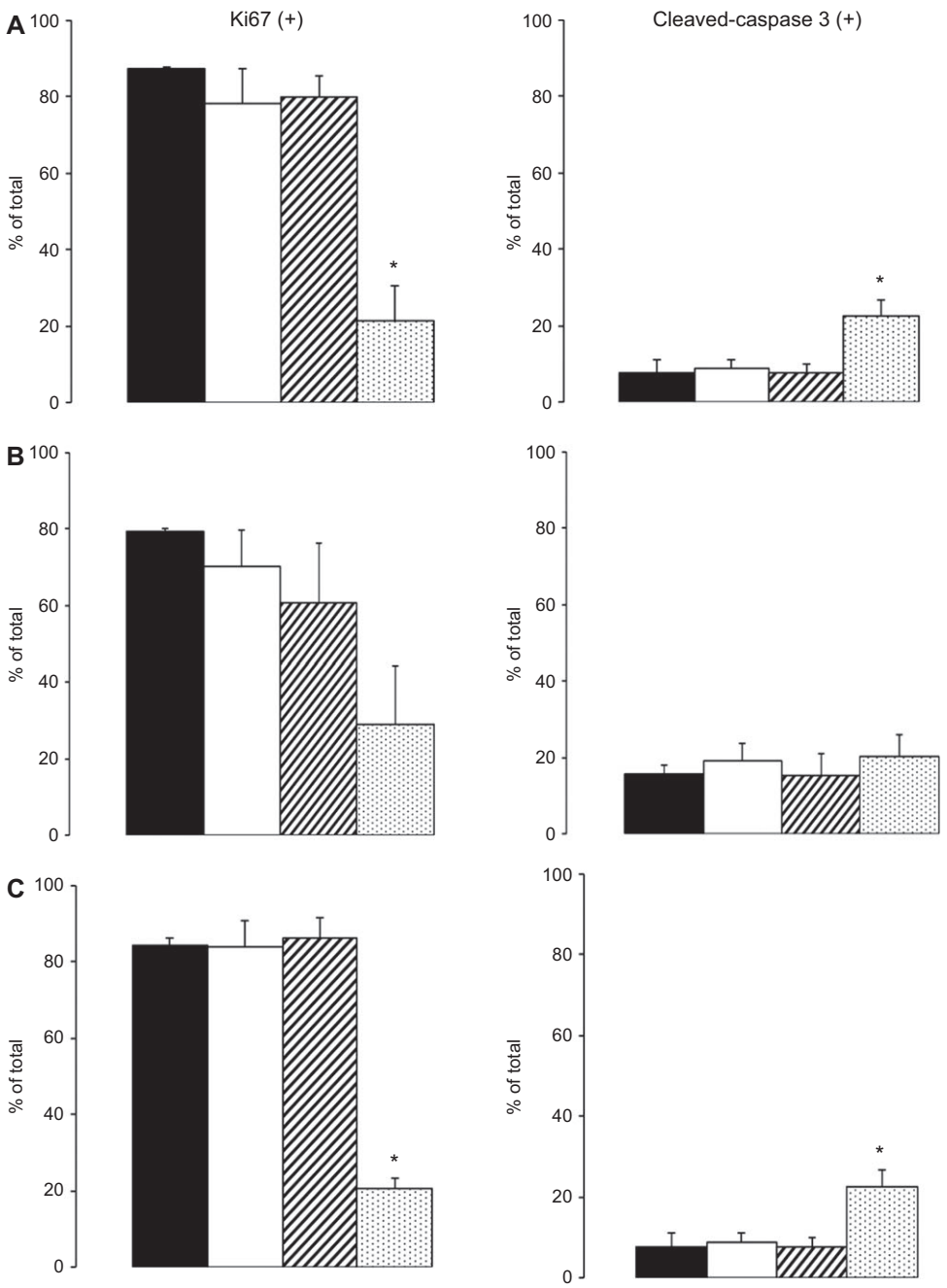

Figure 3 Ki67 staining in MCF10A (A), MCF10AneoT (B) and MCF10AT1 (C) structures is reduced by CA074Me. CA074Me also significantly increased apoptosis in the MCF10A (A) and MCF10AT1 (C) structures. Day 4 structures untreated (black column) or incubated with diluent (0.1% DMSO, white column), 5 μM E64d (striped column) or 5 μM CA074Me (dotted column) were stained for Ki67 or cleaved caspase 3 (right). One hundred structures per treatment group were counted and the percentage of Ki67 (+) or cleaved caspase 3 (+) structures was determined as described in Materials and methods. Mean±SD; *$p<0.01$.

Discussion

We have demonstrated that cysteine cathepsins, and in particular cathepsin B, contribute to the morphogenesis and proliferation of non-transformed and premalignant human breast epithelial cells in 3D rBM overlay cultures. The reduction in structure size and proliferation and increase in apoptosis observed in the presence of the selective cell-permeable CA074Me would be consistent with roles for intracellular cathepsins B and L in these processes. That the broad-spectrum cell-permeable cysteine protease inhibitor E64d was less efficacious

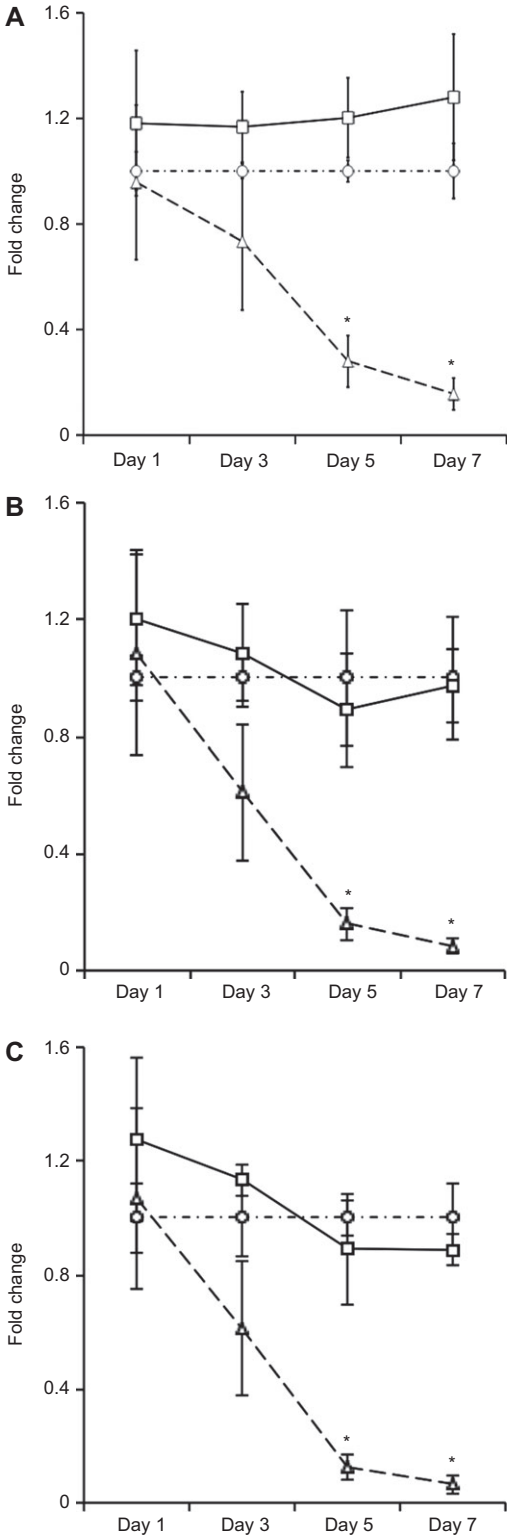

Figure 4 CA074Me decreases proliferation of MCF10A (A), MCF10AneoT (B) and MCF10AT1 (C) cells grown in 3D rBM overlay culture.
Cultures were grown in the presence of 100 μM E64d (□) or 10 μM CA074Me (□) and MTT assays performed on days 1, 3, 5 and 7 post-seeding. Fold change was compared to diluent control [DMSO, (○)]. Mean±SD; *$p<0.001$.

seemed puzzling. To our knowledge, our studies here, using a combination of an ABP (GB111) and immunoprecipitation, are the first to establish that E64d is a less effective inhibitor of cathepsin B than of cathepsin L. The lack of membrane permeability of some inhibitors, e.g., CA074 and E64, does not preclude their eventual uptake via other mechanisms such as endocytosis; nonetheless, these inhibitors did not affect proliferation of the MCF10 variants (Table 1). On the basis of these findings, we conclude that intracellular cathepsin B plays a functional role in the proliferation and premalignant progression of human breast epithelial cells.

The role that cysteine cathepsins play in cell proliferation may differ based on the system analyzed, and is likely complicated by the ability of these proteases to perform redundant functions. Although cathepsin B knockout and cathepsin L knockout mice are both viable, the double knockout of cathepsins B and L is lethal (Felbor et al., 2002), thus supporting functional redundancy of the two proteases. Both cathepsins B and L have been shown to promote cell proliferation and tumor growth in the RIP1-Tag2 transgenic mouse model for pancreatic islet carcinogenesis (Gocheva et al., 2006). In contrast, cathepsin L plays a protective or anti-proliferative role in mouse models for skin cancer, as a deficiency in cathepsin L promotes progression and metastasis (Dennemärker et al., 2010; Benavides et al., 2011). These findings are consistent with studies in cathepsin L knockout mice that demonstrate increased proliferation of keratinocytes caused by altered turnover of EGF and its receptor (Reinheckel et al., 2005). Studies in murine transgenic models for mammary carcinoma have definitively linked cathepsin B to proliferation and progression of these tumors (Vasiljeva et al., 2006, 2008; Sevenich et al., 2011). Interestingly, a recent study in a murine transgenic model for pancreatic ductal adenocarcinoma has established that cathepsin B increases proliferation and progression of these tumors in part by negatively regulating the levels of active cathepsin L (Gopinathan et al., 2012). Although a reduction in cathepsin B activity has been associated with increased apoptosis (Gocheva et al., 2006), others have shown that cathepsin B induces apoptosis (Kroemer and Jaattela, 2005; for a general review on lysosomal cathepsins and cell death, see Repnik et al., 2012). Also of note is that cathepsin X has been shown to compensate for cathepsin B in tumors (for review see, Watson and Kreuzaler, 2009). Clearly, the roles of proteases, including those of cysteine cathepsins, in normal cellular function as well as malignant progression, are complicated. Delineation by multiple techniques of the functions of individual proteases is critically needed if we are to develop therapies targeted against proteases.

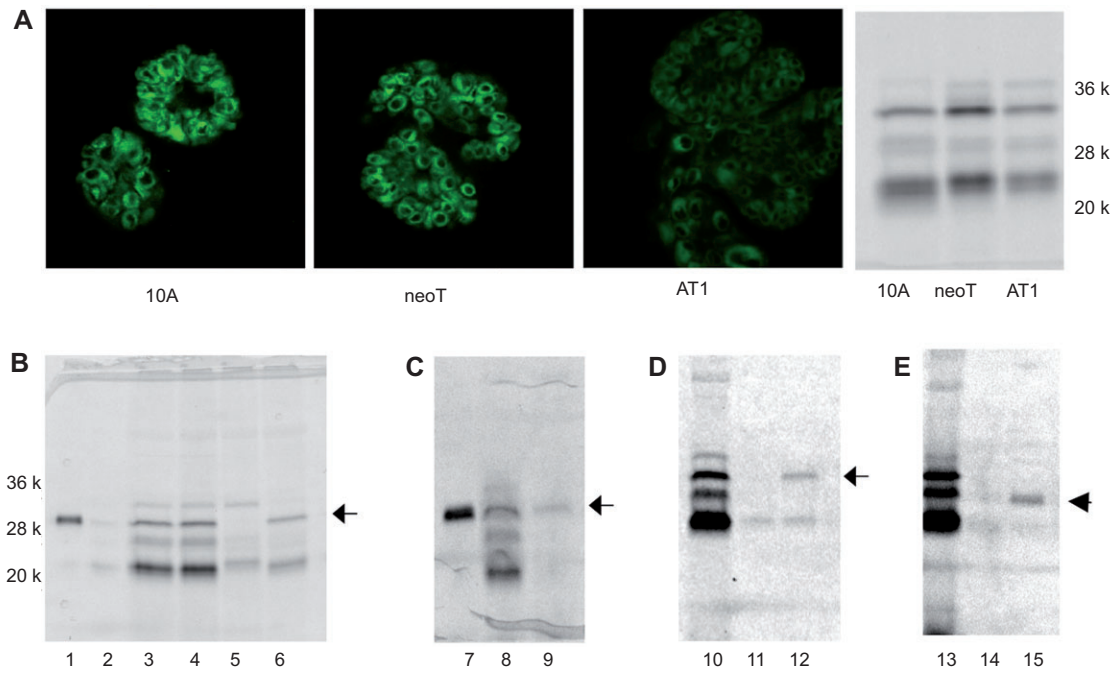

Figure 5 Active cysteine cathepsins in MCF10A variants were imaged and profiled with GB111.
(A) Labeling of cysteine cathepsins is illustrated in optical sections taken at the equatorial plane of representative 12-day 3D rBM overlay cultures. Cultures were incubated with GB111 overnight; unbound probe was removed by washing; and labeled active cysteine cathepsins (green) were imaged with a Zeiss LSM-510 META confocal microscope. Magnification, 40×. Similar bands of active cysteine cathepsins were labeled in the MCF10 variants (A, far right panel). Their identity as cysteine cathepsins was confirmed by inhibition of GB111 binding in MCF10A cells (grown in 3D rBM overlay culture for 4 days prior to overnight incubation with GB111). Controls for these studies were recombinant cathepsin B (lanes 1 and 7); untreated MCF10A cell lysates (lanes 3, 8, 10, and 13); DMSO pretreated MCF10A cell lysate (lane 4); and MCF10A lysates after immunoprecipitation with preimmune IgG (lanes 11 and 14). Experimental lanes represent MCF10A lysates pretreated with 10 μM CA074Me (lane 5); 10 or 100 μM E-64d (lanes 6 and 9, respectively); or subjected to immunoprecipitation with antibodies to cathepsin B (lane 12) or cathepsin L (lane 15). Bands corresponding to cathepsin B and cathepsin L are designated by CB and CL, respectively.

Materials and methods

Materials

Dulbecco's modified Eagles medium/F12, hydrocortisone, insulin from bovine pancreas, BSA, MTT were obtained from Sigma (St. Louis, MO). Antibiotic-antimycotic (100×), Slowfade antifade reagent, and horse serum were from Invitrogen (Carlsbad, CA). Epidermal growth factor was from Upstate Cell Signaling Solutions (Lake, Placid, NY). Cultrex was from Trevigen (Gaithersburg, MD). Phalloidin, Slowfade antifade reagent, and LIVE/DEAD Viability/Cytotoxicity Kits for Animal Cells were from Life Technologies (Grand Island, NY). The CytoTox 96® Non-Radioactive Cytotoxicity Assay Kit was from Promega (Madison, WI); and Protein A/G Plus-Agarose beads were from Pierce (Rockford, IL).

CA-074, CA-074Me, E64, and E64d were purchased from Peptides International (Louisville, KY); GM6001 from Chemicon (Temecula, CA); and PD150606 from Calbiochem (San Diego, CA). GB111 was a kind gift from Dr. Matthew Bogyo (Stanford University, Stanford, CA). SB-3CT was a kind gift from Dr. Shahriar Mobashery (University of Notre Dame, South Bend, IN, USA). Cbz-Phe-Ser(Obzl)-CHN_2, Cbz-Leu-Leu-Tyr-CHN_2, Cbz-Phe-Phe(pNO_2)-CHN_2 and Cbz-Phe-Tyr(OtBu)-CHN_2 were kind gifts from Dr. John Anagli (Banyan Biomarkers, Alachua, FL , USA).

The rabbit anti-human Ki-67 was purchased from Zymed Laboratories (San Francisco, CA, USA); the mouse anti-human CD49f (α6) antibody was from Chemicon (Temecula, CA, USA); the mouse anti-human GM130 was from BD Biosciences (San Jose, CA, USA). The rabbit anti-human cleaved caspase 3 (Asp 175) was from Cell Signaling Technology. The fluorescein-conjugated affinity-purified donkey anti-rabbit IgG, Texas red-conjugated affinity-purified donkey anti-mouse and anti-rat IgG, and normal donkey serum were from Jackson ImmunoResearch (West Grove, PA, USA). Mouse anti-human cathepsin L was a kind gift from Dr. Ekkehard Weber (Martin Luther University Halle-Wittenberg, Halle, Germany). Rabbit anti-human cathepsin B was made and characterized in our laboratory (Moin et al., 1992). All other chemicals were obtained from Sigma (St. Louis, MO, USA).

Methods

Cell lines and culture

MCF10A cells were a kind gift from Dr. Joan Brugge (Harvard University, Cambridge, MA, USA). MCF10AneoT and MCF10AT1 cells were obtained from the Cell Resources Core of the Barbara Ann Karmanos Cancer Institute (Detroit, MI, USA). Isogenic MCF10A variants were

maintained in 2D monolayer cultures in DMEM/F12 supplemented with 5% horse serum, 20 ng/ml EGF, 10 μg/ml bovine insulin, 0.5 μg/ml hydrocortisone and 1× antibiotic-antimycotic. Isogenic MCF10 variants were established in 3D rBM overlay cultures as has been described for MCF10A cells (Li et al., 2008). Briefly, 12-mm round glass coverslips were each coated with 40 μl of ice-cold rBM (Cultrex) and incubated at 37°C for 20 min to allow the rBM to solidify. The coated coverslips were placed in a 24-well plate with the rBM facing up. A trypsinized single cell suspension containing 5000 cells in a 40 μl volume of the assay medium (DMEM/F12 containing 2% horse serum, 5 ng/ml EGF, 0.5 μg/ml hydrocortisone, 10 μg/ml insulin, 50 U/ml penicillin and 50 μg/ml streptomycin, supplemented with 2% (v/v) of Cultrex) was carefully loaded on top of the rBM, and the plate was incubated at 37°C for 30 min to let the cells attach. Then, 500 μl of the assay medium was added per well, and the cells were cultured at 37°C and 5% CO_2, with the medium being changed every 4 days.

Analysis of morphogenetic parameters of 3D rBM overlay cultures

The time-course of morphogenesis of isogenic MCF10 variants in 3D rBM overlay culture was evaluated at 4, 8, 12 and 16 days. Where indicated, inhibitors were added every 48 h to the cultures. Structure size was assessed from equatorial areas of individual structures in ten phase contrast images per cell line that were acquired on a Zeiss Axiophot epifluorescent microscope with a SPOT RT camera using a 40× lens (Gottingen, Germany). Area in pixels was calculated by tracing the outer perimeter of the structure using Adobe Photoshop 7.0 Software.

Structure morphology was assessed by phalloidin staining of the actin cytoskeleton. Structures were fixed with 3.7% formaldehyde for 10 min, permeabilized for 5 min with PBST (PBS with Tween 20) and blocked with 0.2% BSA in PBST for 10 min. Samples were then incubated with phalloidin at a 1:40 dilution in PBST for 1 h, washed with PBST and imaged with a Zeiss LSM-510 META confocal microscope (Gottingen, Germany).

Cell polarity was analyzed by staining for the apical marker GM130 and the basal marker α6 integrin (Debnath et al., 2003). Structures were fixed with 2% paraformaldehyde for 20 min, permeabilized for 5 min with 0.2% Triton X-100 at 4°C, and washed with PBS three times at 10 min/wash. Samples were then blocked for 1 h in IF (immunofluorescent) buffer (130 mM NaCl, 7 mM Na_2HPO_4, 3.5 mM NaH_2PO_4, 7.7 mM NaN_3, 0.1% BSA, 0.2% Triton X-100, 0.05% Tween 20) and incubated with primary antibodies overnight at 4°C. Samples were then washed with IF buffer three times at 20 min/wash and incubated with corresponding secondary antibodies for 2 h at room temperature. This was followed by three washes with IF buffer at 10 min each. Coverslips were then incubated with DAPI in PBS for 10 min, washed three times with PBS and mounted on glass slides with Slowfade antifade reagent. Structures were imaged with a Zeiss LSM-510 META confocal microscope (Gottingen, Germany).

Cathepsin B expression and distribution were analyzed by immunofluorescence staining of the 3D rBM overlay cultures at 4, 8, 12 or 16 days in culture. Cultures were fixed with 2% paraformaldehyde for 20 min or cold methanol for 10 min, permeabilized for 5 min with 0.2% Triton X-100 at 4°C, and washed with PBS three times at 10 min/wash. Samples were then blocked for 1 h in IF buffer (130 mM NaCl, 7mM Na_2HPO_4, 3.5 mM NaH_2PO_4, 7.7 mM NaN_3, 0.1% BSA, 0.2% Triton X-100, 0.05% Tween 20) and incubated with the primary antibody overnight at 4°C. Samples were washed with IF buffer three times at 20 min/wash, incubated with secondary antibody for 2 h at room temperature, followed by three washes with IF buffer for 10 min each. Samples were incubated with propidium iodide in PBS for 10 min, washed three times with PBS and mounted on glass slides with Slowfade antifade reagent. Samples were imaged using a 40× water immersion lens on a Zeiss LSM 510 confocal microscope (Gottingen, Germany).

Cell proliferation and apoptosis assays

Cell proliferation and apoptosis were assessed by staining for a proliferation marker, Ki67, or an apoptotic marker, cleaved caspase 3 (Debnath et al., 2003), following the protocol described above for the polarity markers. MCF10 variants were grown in 3D rBM overlay cultures as previously described (Li et al., 2008) for 4 days and were treated with 0.1% DMSO, 5 μM CA074Me or 5 μM E64d. The percentage of structures that were positive for Ki67 or cleaved caspase 3 was determined by counting a total of 100 structures on two separate coverslips with a Zeiss Axiophot epifluorescent microscope (Gottingen, Germany). Structures were considered Ki67 positive if they contained at least one cell staining for Ki67. Structures were considered to be caspase 3 positive if they contained at least one cell that was positive for cleaved caspase 3 and the positive cell(s) was not localized in the center of a developing lumen.

Proliferation of MCF10 variants in 2D monolayer and 3D rBM overlay cultures was also quantified by MTT assays, which are based on the ability of functional mitochondria in live cells to convert MTT into formazan crystals. The crystals are released by cell lysis and quantified by measuring absorbance at 590 nm with absorbance values being directly proportional to the number of live cells (Alley et al., 1988). For 2D cultures, 1000 cells/well were seeded in 24-well plates. For 3D cultures, cells were seeded as described above. On days 0, 2, 4 and 6, DMSO or the indicated protease inhibitor was added at specified concentrations to wells maintaining the final concentration of DMSO at 0.1% DMSO. On days 1, 3, 5 and 7, cells were incubated with 0.5 mg/ml MTT for 2 h at 37°C. Cells were lysed by adding 500 μl of 20% SDS to each well and incubating overnight at room temperature. Absorbance at 590 nm was measured on a Tecan SpectraFluor Plus plate reader (Mannedorf, Switzerland).

Cell viability/cytotoxicity assays

2D culture: The viability of MCF10 variants in the presence of cysteine protease inhibitors was measured with CytoTox 96® Non-Radioactive Cytotoxicity Assay Kits (Promega, Madison, USA). This assay measures the amount of lactic dehydrogenase release upon loss of plasma membrane integrity. Three $\times 10^5$ cells/well were seeded in 6-well plates. One ml of culture media containing the specified concentration of DMSO or protease inhibitor was added to the cells. Media and lysate samples were collected and assayed according to the manufacturer's instructions. Absorbance at 485 nm was measured on a Tecan SpectraFluor Plus plate reader. 3D culture: Viability of MCF10 variants in 3D rBM overlay culture in the presence and absence of protease inhibitors was measured with a LIVE/DEAD Kit. This assay is based on live cells with esterase activity and an intact membrane

retaining the hydrolysis product of calcein AM, a fluorogenic esterase substrate to a green fluorescent product and dead cells with compromised membranes being permeable to ethidium homodimer-1, a red-fluorescent nucleic acid stain. Cultures were treated with 0.1% DMSO or cysteine protease inhibitors (100 μM E64d or 10 μM CA074Me) every other day for 8 days. Cultures were then washed with PBS (+Mg^{2+} and Ca^{2+}) 3 times and incubated at room temperature with PBS with Mg^{2+} and Ca^{2+} and containing 2 μM calcein AM and 4 μM ethidium homodimer-1 for 30 min. Fluorescence was imaged using a 40× water immersion lens on a Zeiss LSM-510 META confocal microscope (Gottingen, Germany).

Use of ABPs to image and profile active cysteine cathepsins in intact cells

To image active cysteine cathepsins in live MCF10 variants in 3D rBM overlay culture, we grew the cultures for 12 days and incubated with GB111 (1 μM) overnight. The next day we acquired confocal image stacks on a Zeiss LSM-510 META confocal microscope (Gottingen, Germany). To determine the identity of the labeled cysteine cathepsins, cultures were washed four times with PBS and harvested in RIPA buffer (50 mM Tris/HCl, pH 7.4, 150 mM NaCl, 5 mM EDTA, 0.5% deoxycholate and 0.1% SDS). Equal amounts of cell lysate (normalized to 1.6 μg of DNA) were loaded in each lane, proteins separated on 12% SDS-PAGE and labeled active cysteine cathepsins visualized by scanning with a Typhoon (GE Health Care, Piscataway, USA) flatbed laser scanner (Ex/Em 532/580 nm).

The labeled proteases were identified as cysteine cathepsins by reduced binding of GB111 in the presence of cysteine protease inhibitors and by immunoprecipitation with antibodies against cysteine cathepsins. Briefly, MCF10A cells in 3D rBM overlay culture for 4 days were pretreated with 0.1% DMSO or cysteine protease inhibitors (10 or 100 μM E64d or 10 μM CA074Me) for 2 h. GB111 (1 μM) was then added to the culture media. After an overnight incubation with the ABP, cell lysates were prepared as described above and adjusted with RIPA buffer to a volume of 500 μl. Rabbit anti-human cathepsin B or mouse anti-human cathepsin L was added and mixed for 2 h at 4°C, followed by Protein A/G Plus-Agarose beads (30 μl) and mixing overnight at 4°C. Samples were centrifuged at 400×*g* for 2–3 min, supernatant was removed and beads were washed with RIPA buffer and then boiled after addition of 2× sample buffer (20% glycerol, 100 mM Tris/HCl, pH 6.8, 6% SDS, and 10% mercaptoethanol). One ml of cold acetone was added to the supernatant. After 2 h at -80°C, immunoprecipitated proteins were collected by centrifugation at 9300 *g* at 4°C for 30 min, dried and dissolved by boiling in sample buffer. Samples were separated on 12% SDS-PAGE and labeled active cysteine cathepsins visualized by scanning with a Typhoon (GE Health Care, Piscataway, USA) flatbed laser scanner (Ex/Em 532/580 nm).

Statistical analysis

Statistical significance was determined by a two-tailed *t*-test with assumed equal variance. A p value equal to or <0.05 was considered significant.

Acknowledgements: This work was supported by U.S. Public Health Service Grant CA 56586 and a Department of Defense Breast Cancer Center of Excellence (DAMD17-02–1-0693). The Microscopy, Imaging and Cytometry Resources Laboratory was supported by National Institutes of Health Center Grants P30ES06639 and P30CA22453, a Roadmap Grant U54RR020843 and the Perinatal Research Branch of the National Institutes of Health.

Received July 12, 2012; accepted October 4, 2012

References

Abbenante, G. and Fairlie, D.P. (2005). Protease inhibitors in the clinic. Med. Chem. *1*, 71–104.

Alencar, H., Funovics, M.A., Figueiredo, J., Sawaya, H., Weissleder, R., and Mahmood, U. (2007). Colonic adenocarcinomas: near-infrared microcatheter imaging of smart probes for early detection – study in mice. Radiology *244*, 232–238.

Alley, M.C., Scudiero, D.A., Monks, A., Hursey, M.L., Czerwinski, M.J., Fine, D.L., Abbott, B.J., Mayo, J.G., Shoemaker, R.H., and Boyd, M.R. (1988). Feasibility of drug screening with panels of human tumor cell lines using a microculture tetrazolium assay. Cancer Res. *48*, 589–601.

Basolo, F., Elliott, J., Tait, L., Chen, X.Q., Maloney, T., Russo, I.H., Pauley, R., Momiki, S., Caamano, J., Klein-Szanto, A.J. et al. (1991). Transformation of human breast epithelial cells by c-Ha-ras oncogene. Mol. Carcinog. *4*, 25–35.

Benavides, F., Perez, C., Blando, J., Contreras, O., Shen, J., Coussen, L.M., Fischer, S.M., Kusewitt, D.F., Digiovanni, J. and Conti, C.J. (2011). Protective role of cathepsin L in mouse skin carcinogenesis. Mol. Carcinog. *51*, 352–361.

Blum, G., Mullins, S.R., Keren, K., Fonovic, M., Jedeszko, C., Rice, M.J., Sloane, B.F. and Bogyo, M. (2005). Dynamic imaging of protease activity with fluorescently quenched activity-based probes. Nat. Chem. Biol. *1*, 203–209.

Bervar, A., Zajc, I., Sever, N., Katunuma, N., Sloane, B.F., and Lah, T.T. (2003). Invasiveness of transformed human breast epithelial cell lines is related to cathepsin B and inhibited by cysteine proteinase inhibitors. Biol. Chem. *384*, 447–455.

Chen, J., Tung, C.H., Mahmood, U., Ntziachristos, V., Gyurko, R., Fishman, M.C., Huang, P. L., and Weissleder, R. (2002). In vivo imaging of proteolytic activity in atherosclerosis. Circulation *105*, 2766–2771.

Dawson, P.J., Wolman, S.R., Tait, L., Heppner, G.H., and Miller, F.R. (1996). MCF10AT: a model for the evolution of cancer from proliferative breast disease. Am. J. Pathol. *148*, 313–319.

Debnath, J. and Brugge, J.S. (2005). Modelling glandular epithelial cancers in three-dimensional cultures. Nat. Rev. Cancer. *5*, 675–688.

Debnath, J., Muthuswamy, S.K., and Brugge, J.S. (2003). Morphogenesis and oncogenesis of MCF-10A mammary epithelial acini grown in three-dimensional basement membrane cultures. Methods *30*, 256–268.

Dennemärker, J., Lohmüller, T., Mayerle, J., Tacke, M., Lerch, M.M., Coussens, L.M., and Peters, C., Reinheckel, T. (2010). Deficiency for the cysteine protease cathepsin L promotes tumor progression in mouse epidermis. Oncogene *29*, 1611–21.

Felbor, U., Kessler, B., Mothes, W., Goebel, H.H., Ploegh, H.L., Bronson, R.T., and Olsen, B.R. (2002). Neuronal loss and brain atrophy in mice lacking cathepsins B and L. Proc. Natl. Acad. Sci. USA *99*, 7883–7888.

Gocheva, V., Zeng, W., Ke, D., Klimstra, D., Reinheckel, T., Peters, C., Hanahan, D., and Joyce, J.A. (2006). Distinct roles for cysteine cathepsin genes in multistage tumorigenesis. Genes Dev. *20*, 543–556.

Gopinathan, A., Denicola, G.M., Frese, K.K., Cook, N., Karreth, F.A., Mayerle, J., Lerch, M.M., Reinheckel, T., and Tuveson D.A. (2012). Cathepsin B promotes the progression of pancreatic ductal adenocarcinoma in mice. Gut *61*, 77–84.

Guicciardi, M.E., Miyoshi, H., Bronk, S.F., and Gores, G.J. (2001). Cathepsin B knockout mice are resistant to tumor necrosis factor-alpha-mediated hepatocyte apoptosis and liver injury: implications for therapeutic applications. Am. J. Pathol. *159*, 2045–2054.

Halangk, W., Lerch, M.M., Brandt-Nedelev, B., Roth, W., Ruthenbuerger, M., Reinheckel, T., Domschke, W., Lippert, H., Peters, C., and Deussing, J. (2000). Role of cathepsin B in intracellular trypsinogen activation and the onset of acute pancreatitis. J. Clin. Invest. *106*, 773–781.

Joyce, J.A., Baruch, A., Chehade, K., Meyer-Morse, N., Giraudo, E., Tsai, F. Y., Greenbaum, D.C., Hager, J.H., Bogyo, M., and Hanahan, D. (2004). Cathepsin cysteine proteases are effectors of invasive growth and angiogenesis during multistage tumorigenesis. Cancer Cell *5*, 443–453.

Khokha, R. and Werb Z. (2011). Mammary gland reprogramming: metalloproteinases couple form with function. Cold Spring Harb. Perspect. Biol. *3*, 4.

Kleifeld, O., Kotra, L.P., Gervasi, D.C., Brown, S., Bernardo, M.M., Fridman, R., Mobashery, S., and Sagi, I. (2001). X-ray absorption studies of human matrix metalloproteinase-2 (MMP-2) bound to a highly selective mechanism-based inhibitor. Comparison with the latent and active forms of the enzyme. J. Biol. Chem. *276*, 17125–17131.

Korkola, J.E., DeVries, S., Fridlyand, J., Hwang, E.S., Estep, A.L., Chen, Y.Y., Chew, K.L., Dairkee, S.H., Jensen, R.M., and Waldman, F.M. (2003). Differentiation of lobular versus ductal breast carcinomas by expression microarray analysis. Cancer Res. *63*, 7167–7175.

Kroemer, G. and Jaattela, M. (2005). Lysosomes and autophagy in cell death control. *Nat. Rev. Cancer 5*, 886–897.

Li, Q., Mullins, S.R., Sloane, B.F., and Mattingly, R.R. (2008). p21-Activated kinase 1 coordinates aberrant cell survival and pericellular proteolysis in a three-dimensional culture model for premalignant progression of human breast cancer. Neoplasia *10*, 314–329.

Li, Q., Chow, A.B., and Mattingly, R.R. (2010). Three-dimensional overlay culture models of human breast cancer reveal a critical sensitivity to mitogen-activated protein kinase kinase inhibitors. J. Pharmacol. Exp. Ther. *332*, 821–828.

Liu, J., Sukhova, G.K., Yang, J.T., Sun, J., Ma, L., Ren, A., Xu, W.H., Fu, H., Dolganov, G.M., Hu, C. et al. (2006a). Cathepsin L expression and regulation in human abdominal aortic aneurysm, atherosclerosis, and vascular cells. Atherosclerosis *184*, 302–311.

Liu, J., Ma, L., Yang, J., Ren, A., Sun, Z., Yan, G., Sun, J., Fu, H., Xu, W., Hu, C. et al. (2006b). Increased serum cathepsin S in patients with atherosclerosis and diabetes. Atherosclerosis *186*, 411–419.

Lo, A.T., Mori, H., Mott, J. and Bissell, M.J. (2012). Constructing three-dimensional models to study mammary gland branching morphogenesis and functional differentiation. J. Mammary Gland. Biol. Neoplasia. *17*, 103–10.

Lutgens, S.P., Cleutjens, K.B., Daemen, M.J., and Heeneman, S. (2007). Cathepsin cysteine proteases in cardiovascular disease. Faseb J. *21*, 3029–3041.

Martin, K.J., Patrick, D.R., Bissell, M.J., and Fournier, M.V. (2008). Prognostic breast cancer signature identified from 3D culture model accurately predicts clinical outcome across independent datasets. PLoS One *3*, 1–9.

McGowan, E.B., Becker, E., and Detwiler, T.C. (1989). Inhibition of calpain in intact platelets by the thiol protease inhibitor E-64d. Biochem. Biophys. Res. Commun. *158*, 432–435.

Miller, F.R., Soule, H.D., Tait, L., Pauley, R.J., Wolman, S.R., Dawson, P.J., and Heppner, G. H. (1993). Xenograft model of progressive human proliferative breast disease. J. Natl. Cancer Inst. *85*, 1725–1732.

Mohamed, M.M. and Sloane, B.F. (2006). Cysteine cathepsins: multifunctional enzymes in cancer. Nat. Rev. Cancer. *6*, 764–775.

Moin, K., Day, N.A., Sameni, M., Hasnain, S., Hirama, T., and Sloane, B.F. (1992). Human tumour cathepsin B. Comparison with normal liver cathepsin B. Biochem. J. *285*, 427–434.

Montaser, M., Lalmanach, G., and Mach, L. (2002). CA-074, but not its methyl ester CA-074Me, is a selective inhibitor of cathepsin B within living cells. Biol. Chem. *383*, 1305–1308.

Nedvetsky, P.I., Kwon, S.H., Debnath, J., and Mostov, K.E. (2012). cAMP regulates formation of mammary epithelial acini in vitro. Mol. Biol. Cell. *23*, 2973–2980. 2012 Jun 6. [Epub ahead of print].

Obermajer, N., Jevnikar, Z., Doljak, B., and Kos, J. (2008). Role of cysteine cathepsins in matrix degradation and cell signalling. Connect Tissue Res. *49*, 193–196.

Premzl, A., Puizdar, V., Zavasnik-Bergant, V., Kopitar-Jerala, N., Lah, T.T., Katunuma, N., Sloane, B.F., Turk, V., and Kos, J. (2001). Invasion of ras-transformed breast epithelial cells depends on the proteolytic activity of cysteine and aspartic proteinases. Biol. Chem. *382*, 853–857.

Reinheckel, T., Hagemann, S., Dollwet-Mack, S., Martinez, E., Lohmuller, T., Zlatkovic, G., Tobin, D.J., Maas-Szabowski, N., and Peters, C. (2005). The lysosomal cysteine protease cathepsin L regulates keratinocyte proliferation by control of growth factor recycling. J Cell Sci. *118*, 3387–3395.

Reiser, J., Adair, B., and Reinheckel, T. (2010). Specialized roles for cysteine cathepsins in health and disease. J. Clin. Invest. *120*, 3421–3431.

Repnik, U., Stoka, V., Turk, V., and Turk, B. (2012). Lysosomes and lysosomal cathepsins in cell death. Biochim. Biophys. Acta *1824*, 22–23.

Sameni, M., Mullins, S.R., Moin, K., Sloane, B.F., and Osuala, K. (2012). Modeling breast cancer progression in 4D. In:

Breast Cancer Metastasis and Drug Resistance: Challenges and Progress, A. Ahmad, ed. (Springer, New York, in press).

Sevenich, L., Werner, F., Gajda, M., Schurigt, U., Sieber, C., Müller, S., Follo, M., Peters, C., and Reinheckel, T. (2011). Transgenic expression of human cathepsin B promotes progression and metastasis of polyoma-middle-T-induced breast cancer in mice. Oncogene *30*, 54–64.

Seyfried, D.M., Veyna, R., Han, Y., Li, K., Tang, N., Betts, R.L., Weinsheimer, S., Chopp, M., and Anagli, J. (2001). A selective cysteine protease inhibitor is non-toxic and cerebroprotective in rats undergoing transient middle cerebral artery ischemia. Brain Res. *901*, 94–101.

Sloane, B.F. (2012). On How Mammary Gland Reprogramming Metalloproteinases Couple Form with Function. Cold Spring Harb. Perspect. Biol. *4*, p. 7.

Turk, V., Stoka, V., Vasiljeva, O., Renko, M., Sun, T., Turk, B., and Turk, D. (2012). Cysteine cathepsins: from structure, function and regulation to new frontiers. Biochim. Biophys. Acta. *1824*, 68–88.

Vasiljeva, O., Papazoglou, A., Kruger, A., Brodoefel, H., Korovin, M., Deussing, J., Augustin, N., Nielsen, B.S., Almholt, K., Bogyo, M., et al. (2006). Tumor cell-derived and macrophage-derived cathepsin B promotes progression and lung metastasis of mammary cancer. Cancer Res. *66*, 5242–5250.

Vasiljeva, O., Korovin, M., Gajda, M., Brodoefel, H., Bojic, L., Kruger, A., Schurigt, U., Sevenich, L., Turk, B., Peters, C., et al. (2008). Reduced tumour cell proliferation and delayed development of high-grade mammary carcinomas in cathepsin B-deficient mice. Oncogene *27*, 4191–4199.

Wang, B., Sun, J., Kitamoto, S., Yang, M., Grubb, A., Chapman, H.A., Kalluri, R., and Shi, G.P. (2006). Cathepsin S controls angiogenesis and tumor growth via matrix-derived angiogenic factors. J. Biol. Chem. *281*, 6020–6029.

Watson, C.J. and Kreuzaler, P.A. (2009). The role of cathepsins in involution and breast cancer. J. Mammary Gland Biol. Neoplasia *14*, 171–179.

Wilcox, D. and Mason, R.W. (1992). Inhibition of cysteine proteinases in lysosomes and whole cells. Biochem. J. *285*, 495–502.

Wulfkuhle, J.D., Sgroi, D.C., Krutzsch, H., McLean, K., McGarvey, K., Knowlton, M., Chen, S., Shu, H., Sahin, A., Kurek, R., et al. (2002). Proteomics of human breast ductal carcinoma in situ. Cancer Res. *62*, 6740–6749.

Yasuda, Y., Kaleta, J., and Bromme, D. (2005). The role of cathepsins in osteoporosis and arthritis: rationale for the design of new therapeutics. Adv. Drug Deliv. Rev. *57*, 973–993.

Zajc, I., Sever, N., Bervar, A., and Lah, T.T. (2002). Expression of cysteine peptidase cathepsin L and its inhibitors stefins A and B in relation to tumorigenicity of breast cancer cell lines. Cancer Lett. *187*, 185–190.

DOI 10.1515/hsz-2012-0252SUP — Biol. Chem. 2012; 393(12): Ad1–Ad3

Supplemental data

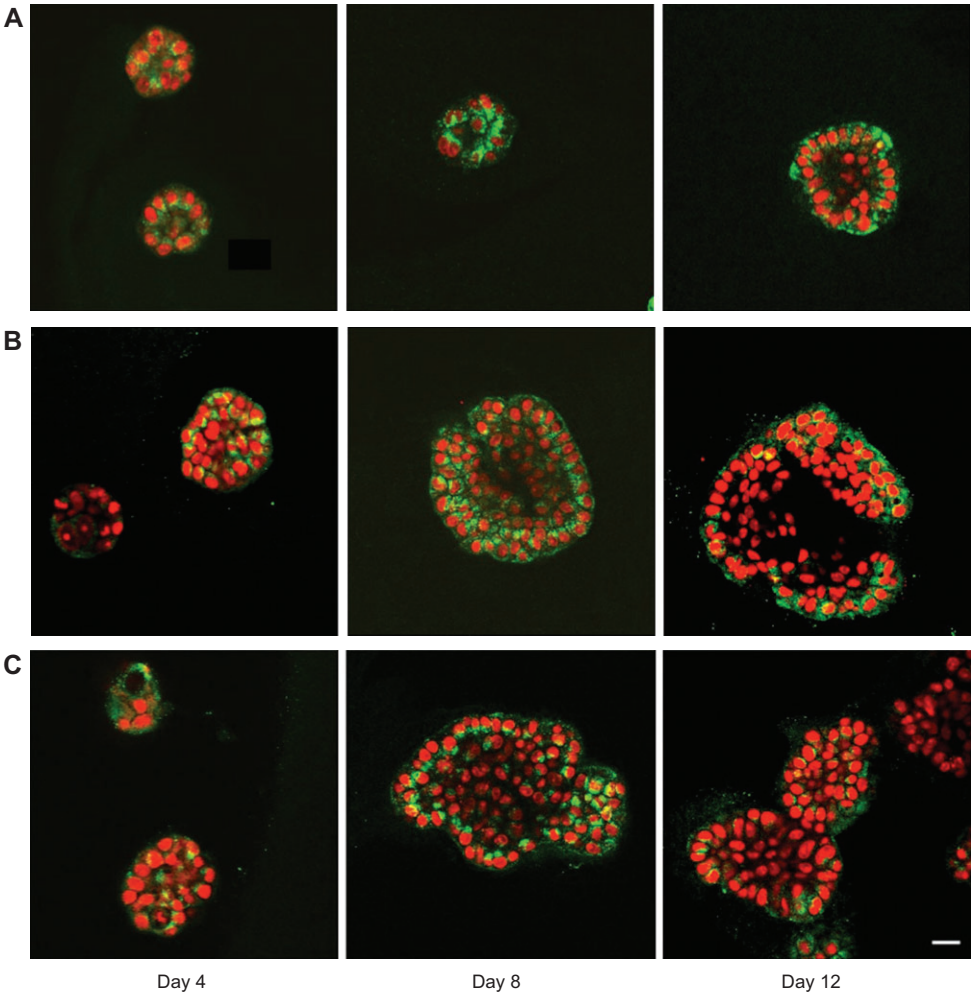

Supplementary Figure 1 Cathepsin B (green) redistributes from the apical to the basal poles of MCF-10A (A), MCF-10AneoT (B) and MCF-10AT1 (C) cells over the course of 12 days in 3D rBM overlay culture. Nuclei were stained with propidium iodide (red). Images represent a single confocal section taken through the equatorial plane of the structures. Bar, 20 μm.

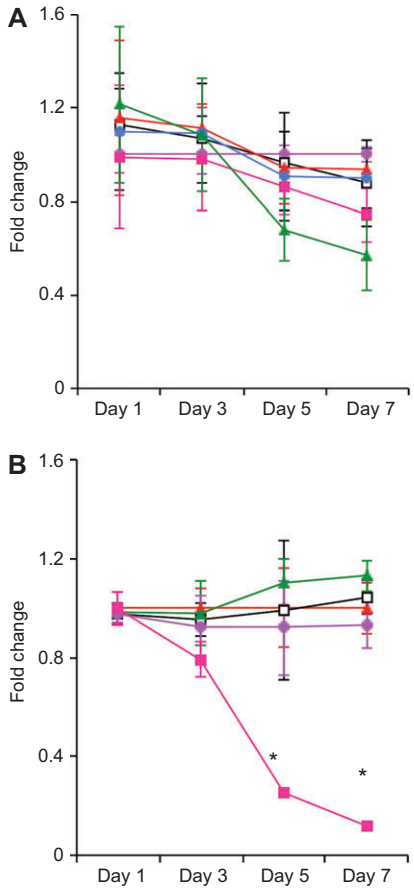

Supplementary Figure 2 CA074Me decreased the proliferation of MCF10 variants grown in 2D monolayer culture. Cells were grown in the presence of 0.01 (□), 0.1 (▲), 1 (●), 10 (■) or 100 (▲) μM E64d (A); or 0.01 (□), 0.1 (▲), 1 (●), 10 (■), or 100 (▲) μM CA074Me (B). MTT assays were performed on days 1, 3, 5 and 7 post-seeding. Fold change was compared to diluent control [DMSO, (○)]. Mean±SD; *$p<0.001$.

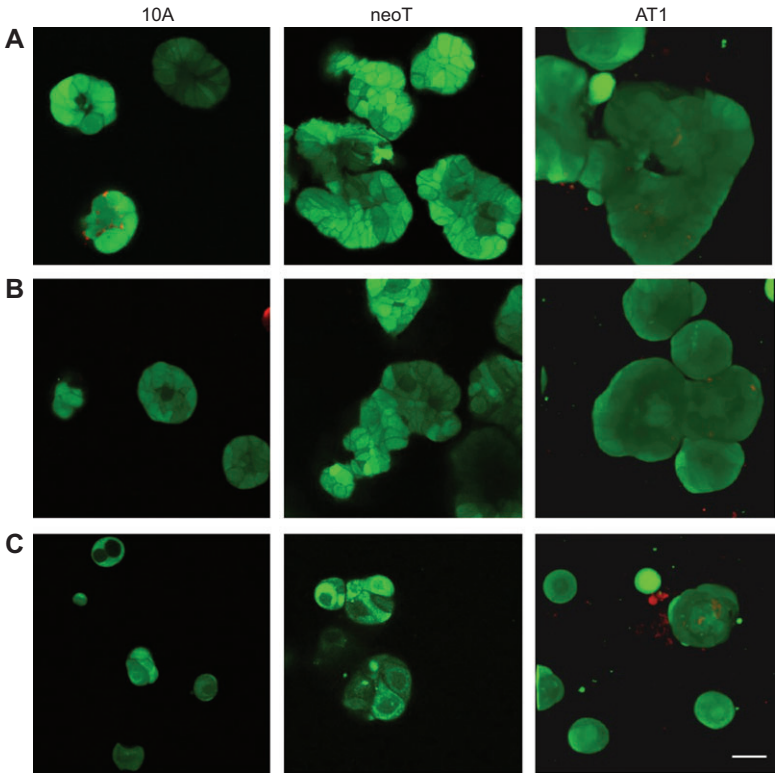

Supplementary Figure 3 E64d and CA074Me did not exhibit general cytotoxicity on MCF10 variants grown in 3D rBM overlay culture. MCF10A, MCF10AneoT and MCF10AT1 cells were cultured for 8 days and treated every other day with 0.1% DMSO (A), 100 μM E64d (B) or 10 μM CA074Me (C). A LIVE/DEAD kit was used to distinguish live (green) and dead (red) cells. Images are representative 3D reconstructions of optical sections acquired through the entire volume of 3D rBM overlay cultures with five fields being analyzed per MCF10 variant. Bar, 20 μm.